Journal of Quantitative Spectroscopy & Radiative Transfer 169 (2016) 104–110

Contents lists available at ScienceDirect

Journal of Quantitative Spectroscopy & Radiative Transfer

journal homepage: www.elsevier.com/locate/jqsrt

Molecular line lists: The ro-vibrational spectra of NaF and KF

Daniel J. Frohman [a], Peter F. Bernath [a,b,*], James S.A. Brooke [b,c]

[a] Department of Chemistry and Biochemistry, Old Dominion University, Norfolk, VA 23529-0126, USA
[b] Department of Chemistry, University of York, Heslington, York YO10 5DD, UK
[c] School of Chemistry, University of Leeds, Leeds LS2 9JT, UK

ARTICLE INFO

Article history:
Received 2 July 2015
Received in revised form
8 October 2015
Accepted 8 October 2015
Available online 20 October 2015

Keywords:
Molecular data
Astronomical data bases
Exoplanets
High temperature systems

ABSTRACT

Rotation–vibration line lists for $^{23}Na^{19}F$, $^{39}K^{19}F$, and $^{41}K^{19}F$ in their ground electronic states are presented. Experimental data previously collected for infrared transitions up to $v=8$ and $v=9$ for KF [1] and NaF [2], respectively, and for pure rotational transitions have been used to construct potential energy curves to yield ro-vibrational energy levels. Dipole moment functions were generated from *ab initio* calculations using the SA-CASSCF and ACPF methods. Full line lists and partition functions are made available as supplementary data.

1. Introduction

There are now more than 1000 confirmed exoplanets, i.e., planets outside our solar system (see exoplanets.com). Many of them are known to be hot rocky super-Earths, with masses between 1 and 10 times that of Earth [3]. The atmospheres of these exoplanets are predicted to contain salt vapors such as NaF and KF [4]. In order to simulate the atmospheric spectra of hot rocky super-Earths, line lists containing line intensities and line positions are needed.

Many experimental and theoretical spectroscopic studies of KF and NaF have been carried out. Early experimental studies from 1963 to 1967 determined ro-vibrational constants, hyperfine constants, and equilibrium dipole moments for NaF and KF [5–10]. An early microwave study on NaF by Bauer and Lew reported $r_e=1.92595(6)$ Å and dipole moments μ for $v=0$, 1, and 2 as 8.19(4) D, 8.29(4) D, and 8.41(4) D, respectively [7,8]. Improved values for the NaF dipole moments were provided by a microwave and radio frequency (rf) study by Hollowell et al., as 8.15576(100) D, 8.22086(100) D, and 8.28670(100) D for $v=0$, 1, and 2, respectively [9]. A fit of these dipole moments to a quadratic expression, Eq. (1), yielded $\mu_e=8.12349(150)$ D, $\mu_I=0.06436(80)$ D, and $\mu_{II}=0.00037(30)$D [9].

$$\mu_v=\mu_e+\mu_I\left(v+\frac{1}{2}\right)+\mu_{II}\left(v+\frac{1}{2}\right)^2 \quad (1)$$

A mm-wave study by Veazey and Gordy provided an updated and expanded set of Dunham parameters for NaF and KF [6]. Van Wachem, et al. calculated μ_e for KF based on fitting μ_v $v=0$ through $v=5$ to Eq. (1), giving $\mu_e=8.558320(800)$ D, $\mu_I=0.068411(40)$ D, and $\mu_{II}=0.000256(7)$ D [10]. Additionally, $\mu_0=8.592478(800)$ D was reported for ^{41}KF [10]. Brumer and Karplus later carried out a theoretical study comparing the accuracy of predicted dipole moments from various models of the electrostatic interactions in alkali halide diatomic species, including KF and NaF [11]. This theoretical study found that their preferred model gave μ_e as 7.6563 D for NaF and 8.5042 D for KF [11]. The prediction of Brumer and Karplus for NaF is an order of magnitude more accurate than that for KF, and our ab initio results show a similar pattern.

More recent experimental and theoretical studies of KF and NaF exist. An *ab initio* study of NaF by Swaminathan

* Corresponding author at: Department of Chemistry and Biochemistry, Old Dominion University, Norfolk, VA 23529-0126, USA.
E-mail address: pbernath@odu.edu (P.F. Bernath).

http://dx.doi.org/10.1016/j.jqsrt.2015.10.004
0022-4073/

and Clementi using an MRCI method provided the potential energy curve and derived rovibrational constants from a Dunham analysis [12]. An additional and similar study by Garcia-Cuesta, et al., computing *ab initio* spectroscopic constants for NaF and KF followed [13]. Spectroscopic constants and a potential energy curve for NaF fitted with existing experimental data were also calculated by Coxon and Hajigeorgiou [14]. A diode-laser high resolution spectroscopic study of NaF by Douay et al., measured the $\Delta v=2$ first overtone band and several hot bands [15]. A global fit of previous microwave data and Douay's measurements using a Dunham analysis provided rovibrational constants and a potential energy curve for NaF [15]. A similar study by Maki and Lovas provides Dunham constants for KF from high resolution spectra of the $\Delta v=2$ band [16].

More recently, improvements to the high-resolution study of NaF were made by Muntianu et al., by recording infrared emission spectra for $\Delta v=1$ bands from $v=0$ to $v=9$ [2]. The infrared study expanded the available Dunham parameters and provides the main experimental data used in our work on NaF [2]. A recent study by Cederberg et al. exists for NaF which provides updated hyperfine constants [17]. Additionally, a recent electron diffraction study of NaF by Wann et al. provides experimental and theoretical bond lengths [18]. Cederberg et al. also carried out a similar study on KF, analogous to the recent NaF hyperfine publication [19]. The most recent high resolution comprehensive infrared emission study of KF is from Liu et al. and is the source of the experimental data used in this study [1]. The KF spectrum was recorded for $\Delta v=1$ bands from $v=0$ to $v=8$ and combined with existing microwave data for a global fit via a Dunham analysis [1]. High quality CCSD(T) calculations of μ_e from Pluta provide values for KF and NaF [20]. Recent comprehensive computational studies of the potential energy curve and the dipole moment function of NaF exist from Giese and York [21]. Giese and York used SA-CASSCF, averaged over the first two $^1\Sigma^+$ states, followed by MRCI calculations [21]. Complete basis set extrapolation values for μ_e and other properties were calculated [21]. However, KF was not present in their study, and so our work adds that species, and conducts calculations for both NaF and KF using an alternative post-SA-CASSCF method, ACPF [22,23]. Additionally, our study makes use of basis sets which are adapted for core electron correlation [24–27], whereas Giese and York [21] used basis sets that only correlated valence electrons [28–30].

2. Method

2.1. Spectroscopic data

The most recent and comprehensive experimental high resolution ro-vibrational transition measurements for KF and NaF are from the infrared work of Liu *et al.* [1] and Muntianu *et al.* [2] respectively. ^{39}KF infrared spectra [1] were recorded at 900 °C for $\Delta v=1$ bands from $v=1\rightarrow0$ to $v=8\rightarrow7$, whereas NaF spectrum [2] was recorded at 1100 °C from $v=1\rightarrow0$ to $v=9\rightarrow8$. Additionally, for NaF 3 microwave [7] and 10 mm-wave [6] lines were used to construct the global line list used for fitting. For ^{39}KF 6 microwave [31, 32] and 14 mm-wave [6] lines were used to construct the global line list.

2.2. Dipole moments

The dipole moments of NaF and KF have been previously studied experimentally by molecular beam electric resonance [7–10,32] as well as with increasingly sophisticated theoretical methods [11,21]. This study contributes new *ab initio* dipole moment functions (DMFs) for both NaF and KF. Calculations were performed using MOLPRO 2012.1. In order to determine the best set of computational parameters with which to calculate the DMFs, μ_e was calculated at previously published r_e values [7,27] for both NaF and KF and compared with experimental μ_e values [7,8,10]. Initially, CASSCF calculations were run with different active spaces, and both with and without state-averaging. When state-averaging was employed, it was over the first two Σ states (the first of which is the $X^1\Sigma^+$ ground state) and used equal weighting. These CASSCF calculations were followed by ACPF calculations. Two different methods for calculation of the dipole moment were used. The first method is to calculate the expectation value at a particular value of r. The second method is the finite field method which calculates the dipole moment as a derivative of the energy with respect to a change in an applied electric field. The first term of the 2 point central difference equation was used which requires calculations at two equal magnitudes but opposite sign field values, Eq. (2) [33,34],

$$E'(0)\approx\frac{E(\lambda)-E(-\lambda)}{2\lambda} \tag{2}$$

Field values used were 0.0003 and −0.0003 a.u. Additionally, CCSD(T)-F12b [35,36] finite field calculations were performed, but found to give μ_e values further from experiment than SA-CASSCF/ACPF, and were not used in the final DMF calculations. Calculated μ_e values from both dipole moment determination methods were compared to the best available experimentally determined μ_e. The calculation method that yielded μ_e closest to the reported experimental value was used to calculate the DMF, Tables S1 and S2. The range of r values for each calculation was determined using the inner and outer turning points from RKR [37] calculations so as to include all values relevant to existing experimental data extrapolated to $v=10$. For both NaF and KF, SA-CASSCF as described above was used for the final DMF calculations. Details unique to the calculations for each molecule are discussed under results.

2.3. Potential energy curves

Potential energy curves (PECs) for NaF and KF were determined by fitting experimental data to various models using computer programs written by R.J. LeRoy. Initially, the program RKR [37] yields potential energy function turning points based on the Rydberg [38,39] -Klein [40] -Rees [41] procedure using experimentally determined Dunham band constants. These RKR [37] turning points up

to v=10 and an *ab initio* dipole moment function (DMF) are used as input for the program LEVEL [42]. LEVEL generates ro-vibrational levels by solving the one-dimensional Schrödinger equation within the Born-Oppenheimer approximation, and provides vibrational transition matrix elements, $\langle\psi_{v'J'}|\mu(r)|\psi_{vJ}\rangle$, that depend on J due to the Herman–Wallis effect [42,43]. BetaFIT [44] used RKR [37] generated potential turning points (Tables S3 and S4) to generate trial values of β_i for the Expanded Morse Oscillator (EMO) potential function, Eqs. (3–5).

$$V_{EMO}(r) = D_e\left[1 - e^{-\beta(r)(r-r_e)}\right]^2 \tag{3}$$

with

$$\beta(r) = \sum_{i=0}^{N_\beta} \beta_i y_p^{eq}(r)^i \tag{4}$$

$$y_p^{eq}(r) = \frac{r^p - r_{eq}^p}{r^p + r_{eq}^p} \tag{5}$$

For both NaF and KF p was chosen as 2. Trial β_i from BetaFIT [44] and a fixed dissociation energy, D_e, are used as input in DPOTFIT to fit the EMO potential function to experimental data [1,2,6,7,31,32]. In addition, a small non-adiabatic correction term, $g(r)$, in the centrifugal potential was included to account for the breakdown of the Born–Oppenheimer approximation (e.g. [45]). The g(r) term is expanded as two polynomials (one for each atom) in the same y variable defined in Eq. (5) using t_i coefficients replacing the β_i's in Eq. (4) [45]. For both NaF and KF, t_1 for F was determined using y_1^{eq} as the expansion variable.

2.4. Line Strength calculations

The line strengths are calculated as Einstein A values, which can be obtained from the following equation [46]:

$$A_{v'J'vJ} = \frac{16\pi^3\nu^3 S_J^{\Delta J}}{3\varepsilon_0 hc^3(2J+1)}\langle\psi_{v'J'}|\mu(r)|\psi_{vJ}\rangle = 3.13618894\times10^{-7}\frac{\tilde{\nu}^3 S_J^{\Delta J}}{(2J+1)}\langle\psi_{v'J'}|\mu(r)|\psi_{vJ}\rangle \tag{6}$$

where ν and $\tilde{\nu}$ are the frequency in Hz and wavenumber in cm^{-1} of the transition, respectively; $\langle\psi_{v'J'}|\mu(r)|\psi_{vJ}\rangle$ is the ro-vibrational transition matrix element (calculated by LEVEL using the fitted potential energy function) in debye, $A_{v'J'vJ}$ in s^{-1}, and $S_J^{\Delta J}$ is the Hönl-London factor, calculated as [47]

$$S_J^{\Delta J} = (-1)^{J'}\sqrt{2J'+1}\sqrt{2J+1}\begin{pmatrix} J' & 1 & J \\ 0 & 0 & 0\end{pmatrix} \tag{7}$$

for the $^1\Sigma$–$^1\Sigma$ transitions considered in this work, where the term on the right-hand side of the equation is a Wigner-3j symbol. Western's PGOPHER [PGOPHER, a Program for Simulating Rotational, Vibrational and Electronic Structure, C.M. Western, University of Bristol, http://pgopher.chm.bris.ac.uk] program was used to calculate Einstein A values and line positions, as it accepts vibrational transition matrix elements as input, and automatically calculates Hönl-London factors and Einstein A values.

The Einstein A values are converted to oscillator strengths (f-values) [46]:

$$f_{v'J'vJ} = \frac{m_e\varepsilon_0 c}{2\pi e^2\nu^2}\frac{(2J'+1)}{(2J+1)}\langle\psi_{v'J'}|\mu(r)|\psi_{vJ}\rangle A_{v'J'vJ} = 1.4991938\frac{1}{\tilde{\nu}^2}\frac{(2J'+1)}{(2J+1)}A_{v'J'vJ} \tag{8}$$

that are present in the final line lists, along with line positions, Einstein A values, and observed positions where available. Transitions were calculated up to $v=10$ for both NaF and KF. These line lists are available as supplemental material.

2.5. Partition functions

In order to estimate accurate partition functions suitable for high temperatures, it is necessary to extrapolate the line list up to high vibrational levels so that all levels with significant contribution to the partition function are included. This is done within LEVEL [42] by selecting values for the limiting parameters which permit convergence of the potential towards the dissociation energy. A maximum J and v must be determined. All levels/states are adjusted to be relative to $v=0, J=0$. Quasibound levels are not included. The Boltzmann factors for all levels/states at a particular temperature are summed to provide the partition function Q as

$$Q = \sum_{v=0}^{v_{max}}\left(\sum_{J=0}^{J_{max}}\left[(2J+1)e^{-E_{vJ}/kT}\right]\right) \tag{9}$$

with v_{max} and J_{max} no greater than 400. Partition functions were calculated for the following temperatures: 9.375, 18.75, 37.5, 75, 150, 225, 300, 500, 750, 1000, 1250, 1500, 1750, 2000, 2250, 2500, 2750, and 3000 K. The partition functions were fitted by multiple linear regression using the expression

$$\log_{10}Q(T) = \sum_{n=0}^{x} a_n\left[\log_{10}T\right]^n \tag{10}$$

from Vidler and Tennyson [49]. Resulting fits for NaF and KF are given in their respective results sections.

3. Results and discussion

3.1. NaF

3.1.1. NaF dipole moment function

The NaF experimental μ_e=8.156(1) D [50] was in closest agreement with the ACPF finite field calculation. The ACPF calculation reference wavefunction came from SA-CASSCF averaged over the ground and first excited $^1\Sigma^+$ states with equal weights, using the aug-cc-pwCV5Z basis set and including outer core correlation. The 1s orbitals of Na and F and the 2s, 2p_x, and 2p_y orbitals of Na were correlated but were kept as closed orbitals in both the SA-CASSCF and ACPF calculations. In the ACPF calculation, the 1s of Na and F are excluded from correlation. The active space used was 4,2,2,0 (a_1, b_1, b_2, a_2) in C_{2v} with NaF r_e set to 1.9259 Å [2,7,51]. The expectation value method and finite field

method of calculating the dipole moment yielded values of μ_e=8.02999 D and 8.13697 D, respectively. A complete basis set (CBS) extrapolation of the μ_e was estimated as 8.13695 D with the CBS extrapolated ACPF finite field total energies calculated at aug-cc-pwCVQZ and aug-cc-pwCV5Z from

$$E(\infty) = E(x-1) + \frac{E(x)-E(x-1)}{1-\left(1-\frac{1}{x}\right)^3},$$

with x=5 due to using the aug-cc-pwCV5Z basis set.

The close agreement between the CBS μ_e and value calculated at aug-cc-pwCV5Z indicates convergence has been achieved at this basis set. In comparison, the Giese and York study find their μ_e in closest agreement with experiment is the $\mu_e CBS^*_{EXP} = 8.029$ D. Similarly, the best value from Pluta for μ_e is 8.128 D. Relative to the experimental μ_e, the expectation value method and finite field method in this study produce percent errors of approximately 1.5% and 0.2%, respectively. A dipole moment curve was calculated for r values from 1.65 Å to 2.40 Å in increments of 0.01 Å over 76 points, approximating the range of turning points calculated via RKR [37] for v up to 10. While the finite field method produces a theoretical μ_e closer to the experimental μ_e than that calculated from the expectation value, the DMF exhibited inappropriate behavior at r values from 1.75 Å to 1.65 Å. When the finite field DMF was plotted, it did not maintain a linear shape in this lower r value range. In contrast, the expectation value method gave an almost linear plot through all r values of interest, and so those values were used as input to LEVEL [42]. From comparison with Giese and York, it appears our DMF will be of similar quality based on the error in μ_e, Table 1.

3.1.2. NaF potential energy curve

The NaF PEC was obtained by fitting 1131 lines using DPOTFIT [47] with D_e fixed to 39,855 cm^{-1}[50] and N_β in Eq. (4) was 4 [2]. The resulting parameters from the fit are presented in Table 2. All line positions were reproduced by the fit within the experimental errors and the DRMSD (dimensionless root mean standard deviation) is 0.4689. The fit potential and the DMF is plotted showing turning points for v=0 to v=10 in Fig. 1. The spectroscopic constants as calculated by LEVEL are provided as Supplementary Table S5.

Table 1
Comparison of calculated μ_e for NaF.

Reference	Method	μ_e/D	μ_e calc-exptl[a]	r_e used[b] (Å)
This Study	SA-ACPF/ expectation	8.02999	−0.12601	1.9259
This Study	SA-ACPF/finite field	8.13697	−0.01903	1.9259
Pluta (2001) [20]	CCSD(T)	8.128	−0.028	1.9259
Giese and York (2004) [21]	SA-MRCI/ expectation[c]	8.029	−0.127	1.921

[a] μ_e=8.156 D, Ref. [36].
[b] r_e=1.9259 Å, Refs. [37,7,15].
[c] Value is from CBS extrapolation method that provided calculated μ_e closest to experimental value.

Table 2
Fitting parameters from DPOTFIT EMO potential fit of NaF and KF.

Parameter	NaF	KF
D_e/cm^{-1}	[39,855.0]	[40,797.0]
r_e/Å	1.92594654(12)	2.17145967(23)
β_0	1.053857615(290)	0.918439203(290)
β_1	−0.5808885(140)	−0.5152726(530)
β_2	0.101274(48)	−0.113146(210)
β_3	0.044970(50)	0.26488(93)
β_4	−0.1077(15)	−0.2508(52)
β_4	–	0.041(20)
$t_1(F)$	$-2.75(71)\times10^{-4}$	$-9.2(32)\times10^{-4}$

Note: Values in square brackets were fixed and 95% confidence interval uncertainties are given in parentheses for the last digits shown.

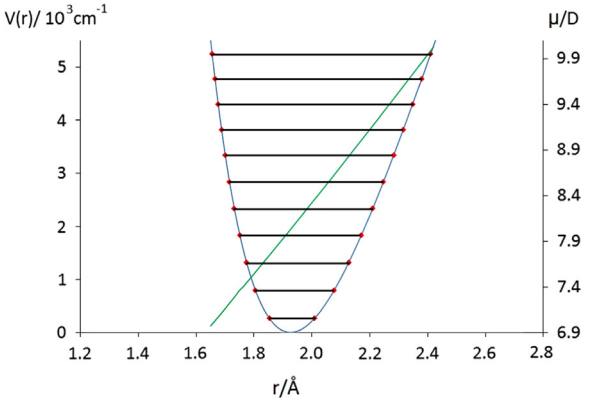

Fig. 1. NaF Extended Morse Oscillator potential with RKR turning points marked up to v=10 and the dipole moment function. The potential is plotted in blue against the left axis and the DMF is plotted in green against the right. Red triangles on the potential indicated RKR turning points from v=0 to v=10. (For interpretation of the references to color in this figure legend, the reader is referred to the web version of this article.)

3.1.3. NaF partition functions

For NaF, the transitions calculated within LEVEL were limited by J_{max}=399 and v_{max}=400. The resulting partition functions calculated up to T=3000 K are presented in Table 3, with comparison where possible with CDMS values [52,53]. The multiple linear regression fit parameters are in Table 4.

3.2. KF

3.2.1. KF dipole moment function

The KF experimental μ_e=8.558320(800) D [10] was in close agreement with the ACPF finite field calculation. As in the NaF calculations, the ACPF reference wavefunction was supplied by a SA-CASSCF calculation equally averaged over the ground and first excited sigma states. Unlike in NaF, the aug-cc-pwCV5Z basis set has not yet been published for K, although the results of calculations making use of it have [27]. The aug-cc-pwCV5Z basis set for K as existing in development was used in all KF calculations with outer core correlation. Both the SA-CASSCF and ACPF

Table 3
Comparison of NaF and KF partition functions from this study with available CDMS values.

Temperature T/K	NaF Q (T)	Q (T) CDMS	KF Q (T)	Q (T) CDMS
9.375	15.3311	15.331	23.7117	23.7118
18.75	30.3245	30.3244	47.0897	47.0898
37.5	60.3218	60.3216	93.8594	93.8594
75	120.3519	120.3516	187.5036	187.5034
150	242.052	242.0513	381.5644	381.5639
225	373.7171	373.7161	603.6254	603.6246
300	523.3633	523.3618	866.4708	866.4697
500	1032.7349	1032.7309	1793.6876	1793.6657
750	1915.3469	–	3440.8681	–
1000	3084.0342	–	5651.6902	–
1250	4549.1916	–	8446.7069	–
1500	6321.1512	–	11847.3587	–
1750	8410.7609	–	15876.5844	–
2000	10829.5663	–	20559.1258	–
2250	13589.9318	–	25921.8215	–
2500	16705.1643	–	31993.9548	–
2750	20189.6579	–	38807.6894	–
3000	24059.0776	–	46398.6188	–

Table 4
Multiple linear regression coefficients for partition function fit using Eq. (10) for NaF.

Parameter	Coefficient
a_0	1.4051649
a_1	−2.545376165
a_2	4.017892376
a_3	−2.158286204
a_4	0.541912807
a_5	−0.04964855

Table 5
Comparison of calculated μ_e for KF.

Reference	Method	μ_e/D	μ_e calc-exptl[a]	r_e used[b] (Å)
This Study	SA-ACPF/ expectation	8.567087	0.008767	2.1782
This Study	SA-ACPF/finite field	8.574362	0.016042	2.1782
Pluta (2001) [20]	CCSD(T)	8.705	0.147	2.1715

[a] μ_e=8.558320(800) D Ref. [10].
[b] r_e=2.1782 Å from a recent high level ab initio value Ref. [22].

calculation restricted the 1*s*, 2*s*, and 2*p* orbitals for K and F, and additionally the 3*s*, $3p_x$, and $3p_y$ orbitals in K, to be closed. In the ACPF calculation, the 1*s* for K and F and the 2*s* and 2*p* for K were excluded from correlation. The active space used was 3,2,2,0 in C_{2v}. An r_e value of 2.1782 Å was used for KF, which was previously calculated at the CCSD (T)/aug-cc-pwCVQZ [27] level. The expectation value and finite field value for μ_e are 8.567087 D and 8.574362 D, respectively, which are both in close agreement to the experimental value with percent errors of 0.1% and 0.2%. These represent an order of magnitude or better agreement with the experimentally determined μ_e than was

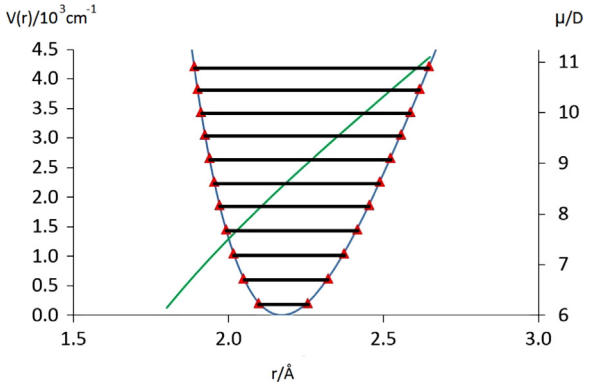

Fig. 2. KF Extended Morse Oscillator potential with RKR turning points marked up to v=10 and the dipole moment curve. The potential is plotted in blue against the left axis and the DMF is plotted in green against the right. Red triangles on the potential indicated RKR turning points from v=0 to v=10. (For interpretation of the references to color in this figure legend, the reader is referred to the web version of this article.)

Table 6
Multiple linear regression coefficients resulting from partition function fit using Eq. (10) for KF.

Parameter	Coefficient
a_0	−2.765334442
a_1	14.1992452
a_2	−22.67858329
a_3	20.78849835
a_4	−10.95585648
a_5	3.310655956
a_6	−0.530343663
a_7	0.034884854

obtained by Pluta [20], Table 5. The CBS estimate for KF is μ_e=8.559133 D and indicates that the calculation using aug-cc-pwCV5Z is approaching convergence. At present, no basis sets of the type aug-cc-pwCVnZ with $n>5$ are available, so it is not known how close to convergence the

next basis set would be. In ^{39}KF the relevant range for r is 1.80 Å–2.65 Å, which approximately corresponds to RKR turning points up to $v=10$. DMF calculations were performed over this range in increments of 0.01 Å over 85 points. Unlike the NaF finite field DMF, there were no deviations from linearity for the finite field method. The finite field method is considered appropriate for methods with limited CI [33,54,55], and since it was without problems for KF, its DMF was used as input to LEVEL [42].

3.2.2. KF potential energy curve

The KF PEC was obtained by fitting to 865 lines using DPOTFIT [48] with D_e fixed to 40797 cm^{-1}[50,51] and N_β in Eq. (4) as 5 [2]. The resulting parameters from the final fit are presented in Table 2. The lines were reproduced within their experimental errors and the DRMSD was 0.9469. A section of the resulting fit potential is shown in Fig. 2 along with the DMF and turning points for $v=0$ to $v=10$ indicated. The spectroscopic constants as calculated by LEVEL are provided as Supplementary Table S6.

3.2.3. KF partition functions

For KF, the transitions calculated within LEVEL were limited by $J_{max}=399$ and $v_{max}=400$. The resulting partition functions calculated up to $T=3000$ K are presented in Table 3, with comparison where possible with CDMS values [52,53]. The multiple linear regression fit parameters are presented in Table 6.

4. Conclusions

Line lists for NaF and ^{39}KF and ^{41}KF have been generated and are provided as Supplementary Tables S7, S8 and S9. For NaF and ^{39}KF experimental data exists with which to compare and illustrate the accuracy of the line lists. The line lists reproduce experimental frequencies to within experimental error. New *ab initio* dipole moments were calculated for NaF and KF up to r corresponding to $v=10$.

Acknowledgments

Support was provided by the NASA Origins of Solar Systems Program (NNX13AI18G). We thank M. Yousefi for help with some of the final fits.

Appendix A. Supplementary material

Supplementary data associated with this article can be found in the online version at http://dx.doi.org/10.1016/j.jqsrt.2015.10.004.

References

[1] Liu M-C, Muntianu A, Zhang KQ, Colarusso P, Bernath PF. Infrared emission spectrum of KF. J Mol Spectrosc 1996;180:188–92.
[2] Muntianu A, Guo B, Bernath PF. High-resolution infrared emission spectrum of NaF. J Mol Spectrosc 1996;176:274–9.
[3] Bernath PF. Molecular opacities for exoplanets. Philos Trans R Soc A 2014:372.
[4] Schaefer L, Lodders K, Fegley Jr. B. Vaporization of the earth: application to exoplanet atmospheres. ApJ 2012;755:41.
[5] Ritchie RK, Lew H. Infrared spectra of NaF and KF. Can J Phys 1964;42:43–52.
[6] Veazey SE, Gordy W. Millimeter-wave molecular-beam spectroscopy: alkali fluorides. Phys Rev 1965;138:1303–14.
[7] Bauer RK, Lew H. Rotational constants and electric dipole moment of NaF. Can J Phys 1963;41:1461–9.
[8] Bauer RK, Lew H. Supplementary note to "rotational constants and electric dipole moment of NaF". Can J Phys 1964;42:830–1.
[9] Hollowell CD, Hebert AJ, Street Jr. K. Radio frequency and microwave spectra of NaF by the molecular beam electric resonance method. J Chem Phys 1964;41:3540–5.
[10] Van Wachem R, De Leeuw FH, Dymanus A. Dipole moments of KF and KBr measured by the molecular beam electric resonance method. J Chem Phys 1967;47:2256–8.
[11] Brumer P, Karplus M. Perturbation theory and ionic models for alkali halide systems. I Diatomics. J Chem Phys 1973;58:3903–18.
[12] Swaminathan PK, Clementi E. Theoretical modeling of NaF: a new configuration interaction potential function and diatomic spectroscopic constants. J Phys Chem 1987;91:1020–3.
[13] Garcia-Cuesta I, Serrano-Andres L, Sanchez de Meras A, Nebot-Gil I. Theoretical spectroscopic parameters of the alkali monofluorides LiF, NaF, and KF. Chem Phys Lett 1992;199:535–44.
[14] Coxon JA, Hajigeorgiou PG. On the direct determination of analytical diatomic potential energy functions from spectroscopic data: the $X^1\Sigma^+$ electronic states of NaF, LiI, CS, and SiS. Chem Phys 1992;167:327–40.
[15] Douay MC, Bopegedera AMRP, Brazier CR, Bernath PF. Diode-laser spectroscopy of alkali halides: the sodium fluoride molecule. Chem Phys Lett 1988;148:1–5.
[16] Maki AG, Lovas FJ. Infrared diode laser spectra of the $\Delta v=1$ Band of AlF and the $\Delta v=2$ Band of KF. J Mol Spectrosc 1982;95:80–91.
[17] Cederberg J, Kang L, Conklin C, Berger E. Hyperfine spectrum of NaF. J Mol Spectrosc 2010;263:142–4.
[18] Wann DA, Rankin DWH, McCaffrey PD, Martin JML, Mawhorter RJ. Equilibrium gas-phase structures of sodium fluoride, bromide, and iodide monomers and dimers. J Phys Chem A 2014;118:1927–35.
[19] Paquette G, Kotz A, Cederberg J, Nitz D, Kolan A, Olson D, et al. The hyperfine spectrum of KF. J Mol Struct 1988;190:143–8.
[20] Pluta T. Nonlinear electric properties of alkali metal halides. Mol Phys 2001;99:1535–47.
[21] Giese TJ, York DM. Complete basis set extrapolated potential energy, dipole, and polarizability surfaces of alkali halide ion-neutral weakly avoided crossings with and without applied electric fields. J Chem Phys 2004;120:7939–48.
[22] Gdanitz RJ, Ahlrichs R. The averaged coupled-pair functional (ACPF): a size extensive modification of MRCI(SD). Chem Phys Lett 1988;143:413.
[23] Werner H-J, Knowles PJ. A comparison of variational and non-variational internally contracted multiconfiguration-reference configuration interaction calculations. Theor Chem Acc 1990;78:175.
[24] Peterson KA, Dunning Jr. TH. Accurate correlation consistent basis sets for molecular core-valence correlation effects: The second row atoms Al–Ar, and the first row atoms B–Ne revisited. J Chem Phys. 2002;117:10548.
[25] Prascher BP, Woon DE, Peterson KA, Dunning Jr. TH, Wilson AK. Gaussian basis sets for use in correlated molecular calculations. VII. Valence and core-valence basis sets for Li, Na, Be, and Mg. Theor Chem Acc 2011;128:69.
[26] Peterson KA. aug-cc-pwCVnZ basis sets for potassium; 2013.
[27] Vasiliu M, Li S, Peterson KA, Feller D, Gole JL, Dixon DA. Structures and heats of formation of simple alkali metal compounds: hydrides, chlorides, fluorides, hydroxides, and oxides for Li, Na, and K. J Phys Chem A 2010;114:4272–81.
[28] Dunning Jr. TH. Gaussian basis sets for use in correlated molecular calculations. I. The atoms boron through neon and hydrogen. J Chem Phys 1989;90:1007.
[29] Feller D. Unofficial basis set from D. Feller available through the Extensible Computational Chemistry Environment Basis Set Database. Version 6/19/03; 2003.
[30] Kendall RA, Dunning Jr. TH, Harrison RJ. Electron affinities of the first-row atoms revisited. Systematic basis sets and wave functions. J Chem Phys 1992:96.
[31] Green GW, Lew H. Can J Phys 1960;38:482.
[32] Dijkerman H, Flegel W, Gräff G, Mönter B. Z Naturforschung A 1972;27:100.

[33] Lodi L. Theoretical rotational-vibrational spectroscopy of water. London: University of London; 2008.
[34] Conte SD, de Boor C. Elementary numerical analysis. 3rd ed. New York: McGraw-Hill; 1980.
[35] Adler TB, Gerald K, Werner H-J. A simple and efficient CCSD(T)-F12 approximation. J Chem Phys. 2007;127:221106.
[36] Adler TB, Werner H-J. Local explicitly correlated coupled-cluster methods: efficient removal of the basis set incompleteness and domain errors. J Chem Phys 2009;130:241101.
[37] Le Roy RJ. RKR1. 2.0 ed. Waterloo, Ontario: University of Waterloo; 2004.
[38] Rydberg R. Z Phys 1931;73:376.
[39] Rydberg R. Z Phys 1933;80:514.
[40] Klein O. Z Phys 1932;76:226.
[41] Rees ALG. Proc Phys Soc 1947;59:998.
[42] Le Roy RJ. Level. 8.2 ed. Waterloo, Ontario: University of Waterloo; 2014.
[43] Herman R, Wallis RF. Influence of vibration-rotation interaction on line intensities in vibration-rotation bands of diatomic molecules. J Chem Phys 1955;23:637–46.
[44] Le Roy RJ. betaFit. 2.1 ed. Waterloo, Ontario: University of Waterloo; 2013.
[45] Henderson RDE, Shayesteh A, Tao J, Haugen CC, Peter F, Bernath PF, et al. Accurate analytic potential and Born-Oppenheimer breakdown functions for MgH and MgD from a direct-potential-fit data analysis. J Phys Chem A 2013;117:13373–87.
[46] Bernath PF. Spectra of atoms and molecules. Third ed. Oxford University Press; 2016.
[47] Brown J, Carrington A. Rotational Spectroscopy of Diatomic Molecules.New York: Cambridge University Press; 2003.
[48] Le Roy RJ. DPOTFIT. 2.0 ed. Waterloo, Ontario: University of Waterloo; 2013.
[49] Vidler M, Tennyson J. J Chem Phys 2000;113:9766.
[50] Haynes WM, editor. CRC handbook of chemistry and physics. 95th ed. Boca Raton, FL: CRC Press/Taylor and Francis; 2015.
[51] Huber KP, Herzberg G. Molecular spectra and molecular structure constants of diatomic molecules.New York: Van Nostrand; 1979.
[52] CDMS. NaF, $\nu=0,1$. CDMS. p. CDMS catalog entry for NaF.
[53] Muller HSP, Schloder F, Stutzki J, Winnewisser G. The Cologne database for molecular spectroscopy, CDMS: a useful tool for astronomers and spectroscopists. J Mol Struct 2005;742:215–27.
[54] Lipinski J. On the consequences of the violation of the Hellmann–Feynman theorem in calculations of electric properties of molecules. Chem Phys Lett 2002;363:313–8.
[55] Ernzerhof M, Marian CM, Peyerimhoff SD. On the calculation of 1st-order properties – expectation values versus energy derivative approach. Internat J Quant Chem 1992;43:659–68.